# Validation report

Release 2026


## City-Level Adaptive Resilience Applications

Revision 1

# Wind patterns in urban spaces

When it comes to urban planning and policy making, knowledge of wind flow patterns around buildings is extremely important. The size and shape of a building plays an important role in locally modifying the wind flow in a region. Wind flow in an urban canopy is generally dictated by the Atmospheric Boundary Layer (ABL). The ABL is a velocity profile region below the stratosphere that is significantly affected by earth's surface. It generally extends from the earth's surface up to a height of about 1-2 km (see Fig.1).

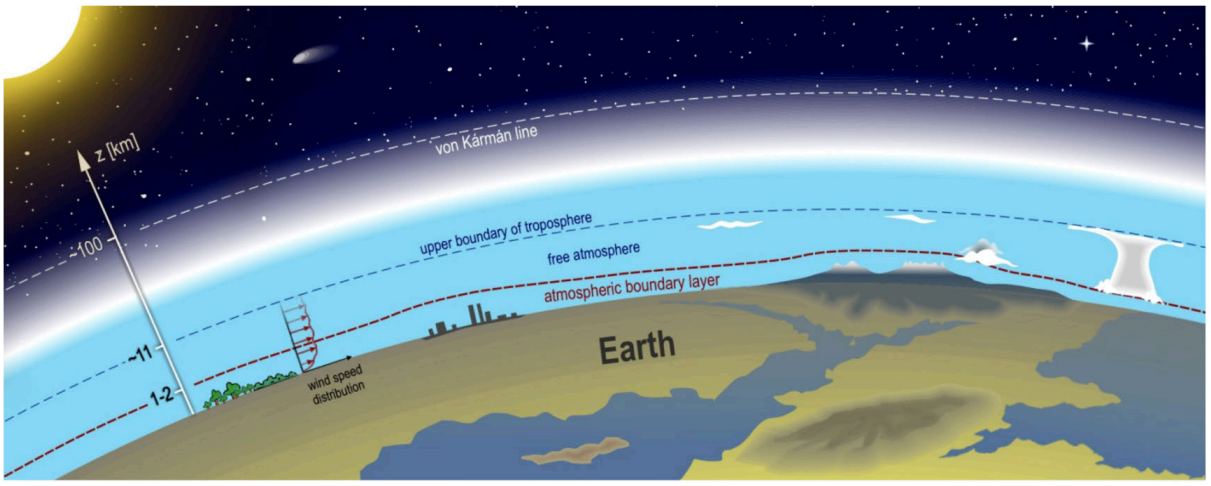


Figure. 1: Atmospheric Boundary Layer (ABL). Image source: Budapest University of Technology and Economics (BME)

The presence of buildings close to the earth's surface significantly changes the velocity magnitudes and directions of the ABL profile. These changes can both be beneficial and disadvantageous: a building may create a favorable urban wind environment or worsen it. Often, the presence of buildings create complex flow patterns in their vicinity. Some of the most common wind patterns around buildings include :

## Downwash effect

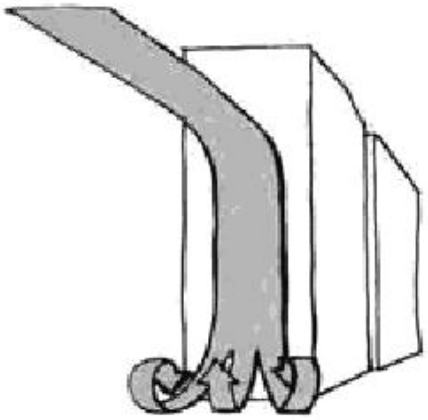

Figure. 2: Downwash effect [Bennet., 2007]

This effect occurs typically in front of tall buildings or towers. Wind speed generally increases with height because of the presence of a boundary layer. When a tall tower obstructs such a boundary layer, higher pressure is created at the top compared to its base. This difference in pressure forces the wind to flow downwards and rollup as shown in Fig. 2, creating higher turbulent winds at pedestrian levels.

## Corner effect

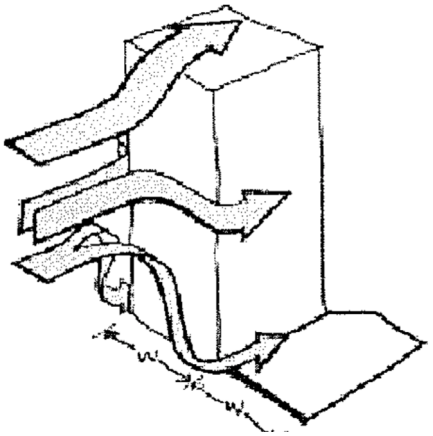

Figure. 3: Corner effect [Bennet., 2007]

This effect occurs when the wind is forced to flow around the corners of buildings. The high pressure winds from the windward side are accelerated around the corners to move towards the low pressure leeward sides of the buildings, thereby increasing the speeds near the corners.

# Wake effect

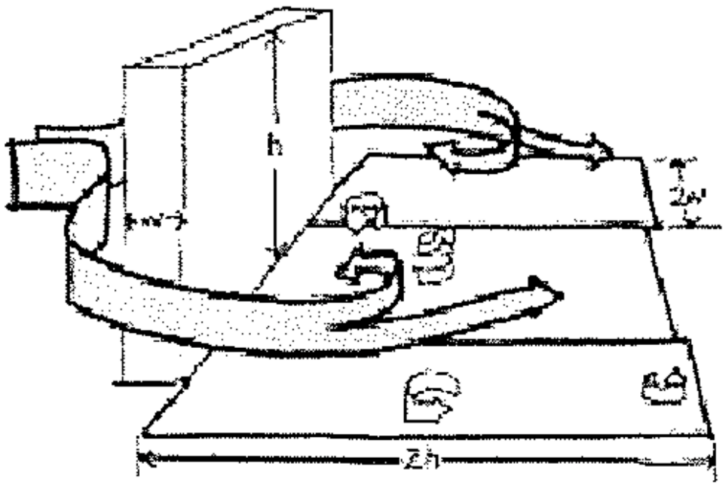


Figure. 4: Wake effect [Bennet., 2007]

This effect is generally a consequence of the previously mentioned corner effect. The wind accelerated around the corners is highly turbulent and three-dimensional that creates zones of recirculation in the wake of the buildings.

The above discussed effects are due to single, isolated buildings. But in an urban environment, that is rarely the case. When there are groups of buildings in a region, these effects combine and can cause undesirable wind speeds at different heights. Some examples include:

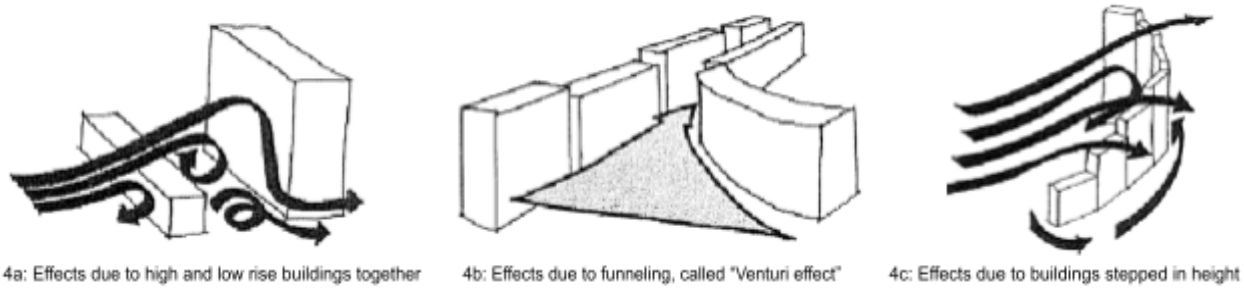


Figure. 5: Cumulative effects of grouped buildings [Bennet., 2007]

The readers are referred to (Bennet., 2007) for a more comprehensive discussion of such effects.

From these examples, it is obvious that the local wind speeds in an urban setting are highly inhomogeneous and are affected by the location, size, and shape of the buildings. These wind speeds and patterns also depend on urban climatology. A correct assessment of speeds in urban areas is nowadays highly recommended in order to help urban planners and policymakers to make better decisions for the urban environment.

# CFD: a tool for wind engineering

Computational fluid dynamics (CFD) is a powerful tool that can be used to study the behavior of fluids, including air, in a wide range of applications. It can be used to study the flow of air around buildings and other structures. Many well-established standards for wind comforts such as NEN8100 [NEN8100., 2006], London microclimate guidelines [London guidelines., 2019] have incorporated the use of numerical simulations using CFD to perform a wind comfort study. The results of a CFD simulation can be used to assess the impact of complex wind flow patterns on comfort and safety for people, on energy harvesting using wind turbines, on wind loads. For example, the simulation can be used to identify areas where strong gusts of wind happen or where wind-induced turbulence might generate issues. The results of the simulation can also be used to design a specific building and its surrounding environment to minimize the impact of wind.

## Advantages of using CFD over wind tunnel testing

In recent years, with the ever increasing computational resources at hand, many architects and engineers prefer using numerical simulations over the traditional windtunnel testing to study wind flow around buildings. There are several advantages to using CFD instead of wind tunnel testing for studying building aerodynamics:

1. **Cost**: CFD simulations can be much less expensive than wind tunnel testing, especially for large or complex structures. This is because wind tunnel testing requires the construction of a physical scale model, which can be costly and time-consuming. CFD simulations, on the other hand, can be run on a computer, eliminating the need for a physical scale model.
2. **Flexibility**: CFD simulations can be easily modified to study different wind conditions or design variations, whereas wind tunnel testing requires the construction of a new physical scale model for each variation. This makes CFD a more flexible and efficient tool for studying building aerodynamics.
3. **Accuracy**: CFD simulations can provide more accurate and detailed results than wind tunnel testing, especially for complex or irregular structures. This is because CFD simulations can model the flow of air around the structure with greater precision, whereas wind tunnel testing relies on the use of scale models, which may not accurately reproduce the flow of air around the full-scale structure.
4. **Speed**: CFD simulations can be run much faster than wind tunnel testing, especially for large or complex structures. This allows engineers to quickly analyze and optimize the design of the building for wind resistance and energy efficiency.
5. **Data**: With CFD simulations, one can have more information in terms of the entire 3D grid around the region of interest, whereas with wind tunnel tests, most often the information is only obtained on a plane or a few points of interest in the domain

# CFD methodology

The method of CFD involves numerically solving a set of differential equations called the Navier-Stokes (NS) equations [Anderson et al., 1995] that describe the motion of fluids. They are based on the principles of conservation of mass, momentum, and energy, and they describe how the velocity, pressure, density, and temperature of a fluid change over time and space.

In the context of atmospheric flows such as flow around buildings, these equations take a specific form called the Reynolds Averaged Navier-Stokes (RANS) equations [Anderson et al., 1995]. They are ensemble-averaged versions of the original NS equations and are used to describe fluid flows that are turbulent in nature. Specifically for wind simulations, the equations usually take up the form of steady (does not vary in time), incompressible (air density is constant) RANS equations. There are a variety of models that solve these RANS equations, which differ by the closure approach used to model the turbulent stresses. The readers are referred to [Pope., 2000; Ferziger et al., 2002]. CLARA uses the well-established **k-ω SST** model [Menter., 1994] that has been proven to be very accurate for predicting flows involving adverse pressure gradients and flow separation [Menter., 2003]. It is a two-equation model that solves additional equations for turbulent kinetic energy (**k**) and specific dissipation rate (ω) to model the turbulent stresses.

It is also very important to use an appropriate Atmospheric Boundary Layer (ABL) model to get accurate near wall velocities. The ABL is the region below the stratosphere that is significantly affected by earth's surface. There have been numerous reports in literature [Blocken et al., 2007; Hargreaves et al., 2007; Parente et al., 2011] that discuss the effects of using an inconsistent ABL model. The most direct consequence is the artificial acceleration of wind velocities very close to the ground (see Fig. 6). Especially when performing simulations in urban areas, this acceleration would result in a significantly worse wind map of the city. An example of a case study that gets affected by an improper ABL model is shown in the later section.

To perform a better and an accurate wind comfort study, CLARA utilizes an improved ABL model [Bellegoni et al., 2023; Srikumar et al., 2024] that is fully consistent with the **k-ω** SST RANS model, based on the previous works of Parente *et al*. This improved ABL model consists of modifications introduced to the turbulent wall functions, as well as to the **k** and ω equations. The entire description of the model is detailed in Bellegoni *et al*.

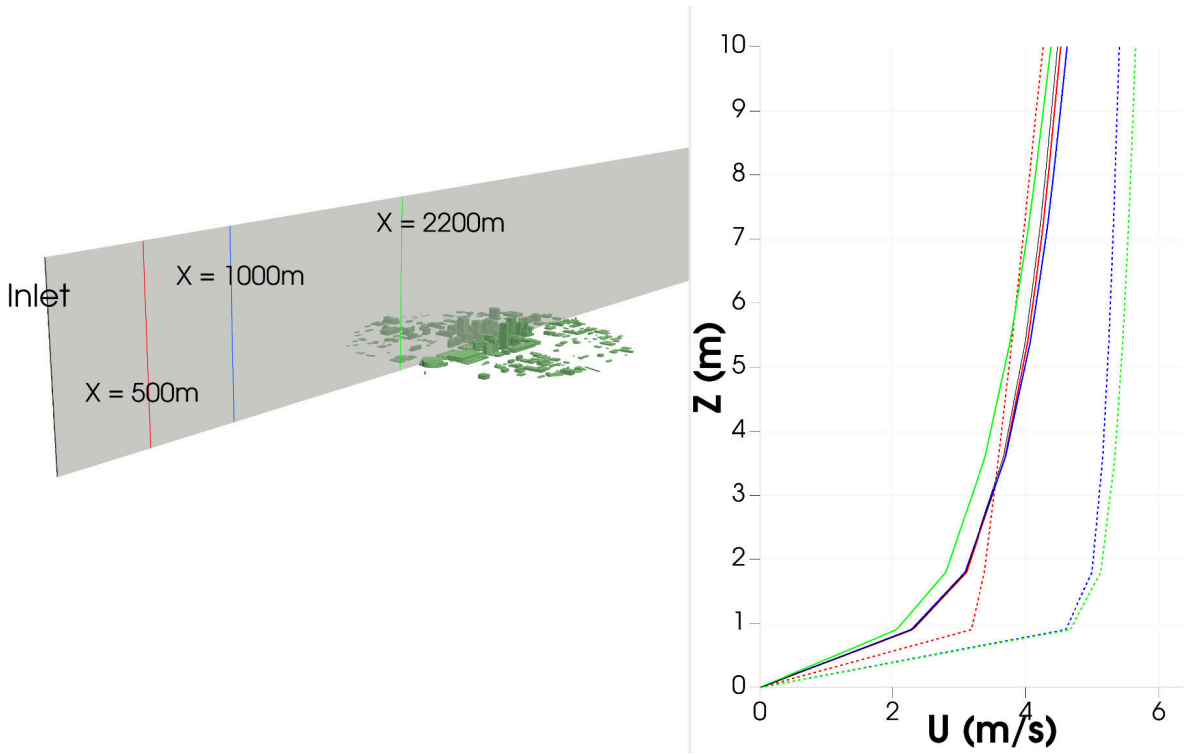


Figure. 6: Acceleration of near-ground velocities due to improper ABL model. Here solid line denotes the improved ABL model, and dashed-line denotes the incorrect ABL model.

# Wind simulations using CFD

Performing wind simulations of urban locations requires two main pieces of information:

- **Statistical meteorological data**: statistical wind data from a nearby meteorological station, usually covering a period of 30 years;
- **Aerodynamic information**: the local roughness data used to transform the meteorological wind data to the area of interest.

## Statistical meteorological data

These are the steps involved to properly utilize the meteorological data to set the inlet velocity conditions for the CFD domain:

1. Firstly, the hourly averaged wind data are obtained from the nearest weather/meteorological station for the area of interest, usually at a height of about 10m from the ground. The weather station should ideally be located on an open flat terrain, such as an airport, that has an equivalent aerodynamic roughness of $z_0$ = 0.03m [Wieringa., 1992]. As mentioned previously, to get reliable statistics in each wind direction, the data should typically cover a period of a few decades.

2. The mean wind velocity obtained from the weather station needs to be transformed to a reference height from the ground [WMO., 1996]. NEN8100 [NEN8100., 2006] typically suggests a reference height of 60m. This transformation is done as follows:

   ➢ A logarithmic law is assumed for the wind profile, given as:

   $$u(z) = \frac{u^*}{\kappa} ln\left(\frac{z+z_0}{z_0}\right)$$

   with $z_0$ denoting the aerodynamic roughness, $u$ * referring to the friction velocity, $\kappa$ is the von Karman constant and $z$ is the vertical coordinate

   ➢ $$\frac{u(60m)}{u(10m)} = \frac{ln\left(\frac{60+z_0}{z_0}\right)}{ln\left(\frac{10+z_0}{z_0}\right)}$$

   Substituting $z_0$ of the terrain at the weather station, one can obtain the velocity at $z = 60m$

3. The obtained reference velocity at 60m is taken as the reference velocity at the inlet of the CFD domain. Again, assuming the logarithmic profile for the velocity, $u$ * to be set at the inlet is calculated from the reference velocity and $z_0$ at the inlet.

# Aerodynamic information

It is important to specify the correct local roughness at the inlet of the domain as well as on the ground within the domain to get accurate behavior of the ABL. The most commonly used classification for the roughness of different terrain types is the one introduced by Wieringa *et al*. This classification is adopted to specify the roughness of the terrain in and around the explicitly modeled buildings. Outside this region, the classification and method mentioned in the Eurocode [Gulvanessian., 2001] is adopted, since it takes a more conservative approach of roughness specification such that the worst case scenario is automatically taken into account for wind comfort.

| Terrain category | z0 (m) |
|---|---|
| **0** Sea or coastal area exposed to the open sea | 0.003 |
| **I** Lakes or flat and horizontal area with negligible vegetation and without obstacles | 0.01 |
| **II** Area with low vegetation such as grass and isolated obstacles (trees, buildings) with separations of at least 20 obstacle heights | 0.05 |
| **III** Area with regular cover of vegetation or buildings or with isolated obstacles with separations of maximum 20 obstacle heights (such as villages, suburban terrain, permanent forest) | 0.3 |
| **IV** Area in which at least 15 % of the surface is covered with buildings | 1.0 |

Table 1: Roughness classification from Eurocode [Gulvanessian., 2001]

| Classification | Landscape | z0 (m) |
|---|---|---|
| sea | sea, paved areas, snow-covered flat plain, tide flat, smooth desert | 0.0002 |
| smooth | beaches, pack ice, morass, snow-covered fields | 0.005 |
| open | grass prairie or farm fields, tundra, airports, heather | 0.03 |
| roughly open | cultivated area with low crops and occasional obstacles (single bushes) | 0.1 |
| rough | high crops, crops of varied height, scattered obstacles such as trees or hedgerows, vineyards | 0.25 |
| very rough | mixed farm fields and forest clumps, orchards, scattered buildings | 0.5 |
| closed | regular coverage with large size obstacles with open spaces roughly equal to obstacle heights, suburban houses, villages, natural forests | 1.0 |
| chaotic | centers of large towns and cities, irregular forests with scattered clearings | Greater than or equal to 2 |

Table 2: Roughness classification from Wieringa [Wieringa., 1992]

The procedure to specify roughness using the Eurocode method is detailed below:

- Take the max height among the explicitly modeled buildings as H. Compute the Eurocode roughness circle radius as $R_{euro} = max(23H^{1.2}, 300)$.
- Draw the three circles corresponding to the Eurocode circle, domain extent and the context extent (i.e. the area enclosing the explicitly modeled buildings). An example is shown in Fig.7.
- Divide the circles into 12 sectors of 30 deg each as shown in Fig.7 .
- To assign the roughness value at the inlet for each sector, take the area enclosed between the Eurocode circle and domain inlet of a particular sector, and compute the least roughness with an area > 10% of the considered sector according to the Eurocode classification shown in Table 1. The obtained roughness value is assigned to the corresponding inlet direction. Perform the same for all the 12 sectors and get the roughness values to be assigned at the domain inlet for each direction.
- To assign the roughness values for the terrain between the inlet and the context, take the area enclosed between the domain inlet and the context of a particular sector and perform the same steps as explained previously.

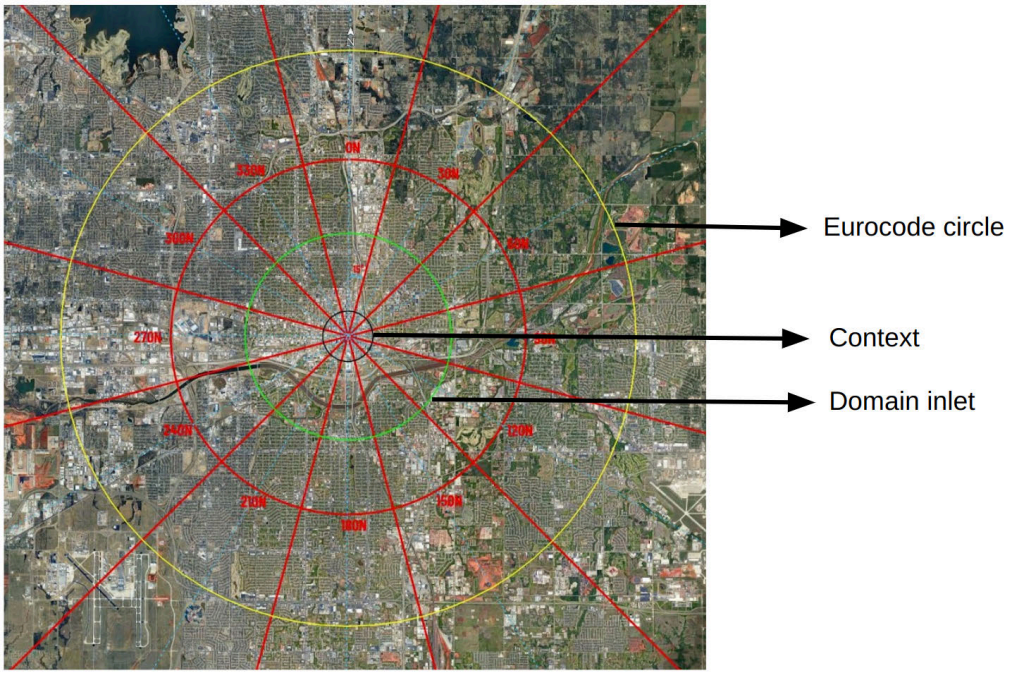


Figure. 7: Roughness specification method using Eurocode

For the terrain roughness values within the context area, it should be noted that since the buildings are explicitly modeled, only the roughness corresponding to the ground must be specified. This is unlike what is described above for the regions outside the context, since these regions have no explicitly modeled buildings in the CAD, the effect of the buildings on the flow is

only seen through the roughness values. Thus for the context area, the sector-wise roughness is defined through the Davenport & Wieringa classification shown in Table 2.

# Meshing and simulations

A computational mesh is used in CFD simulations to discretize the fluid domain and solve the governing equations of fluid flow numerically. The mesh is made up of small, interconnected elements, such as tetrahedrons or hexahedrons, that approximate the geometry of the fluid domain. The accuracy and resolution of the simulation depends on the size and distribution of these elements. The use of a computational mesh allows for the simulation of complex fluid flows that would be difficult or impossible to solve analytically.

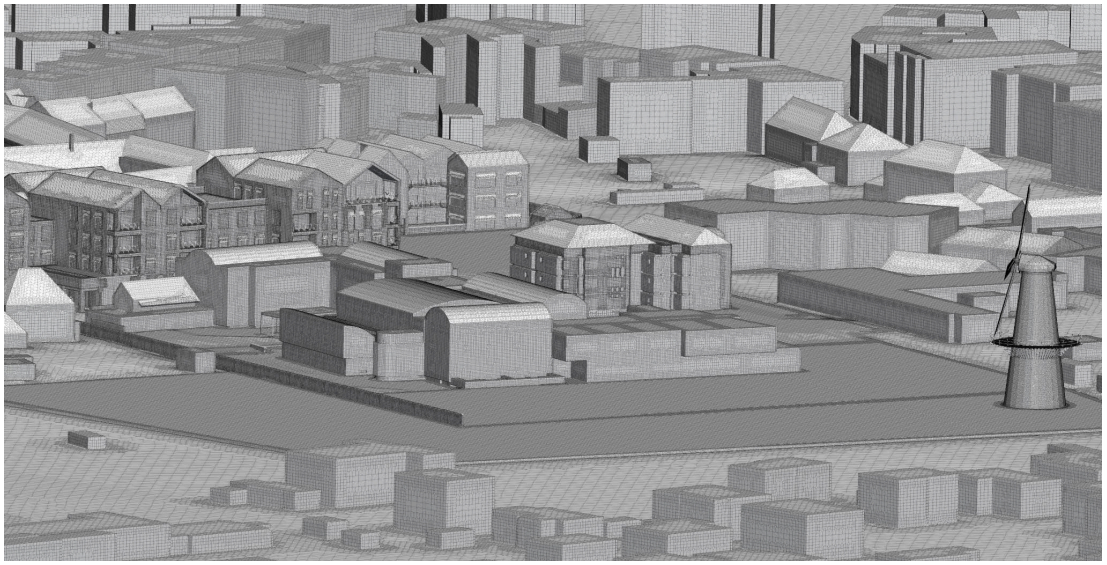

Figure. 8: An example of a computational used for CFD simulations

It is of paramount importance to use a proper mesh with satisfactory resolution to obtain any reliable results. A summary of relevant guidelines in the context of building simulations to obtain a good mesh are curated from the COST guidelines [Franke et al., 2010], NEN8100 [NEN8100., 2006] and Blocken [Blocken., 2015] is given below:

- Within the region of interest, all geometrical details of buildings with size > 1m must be included
- The minimum grid resolution for the built area should be at least 10 cells per cube root of the building volume and 10 cells per building separation
- Computational domain extents : The top of the domain should be at least 5H distance away from the maximum height of the buildings H. The lateral boundaries and the inlet should be at least 5H distance away from the region of the context. Outlet should be placed at least 15H away from the context

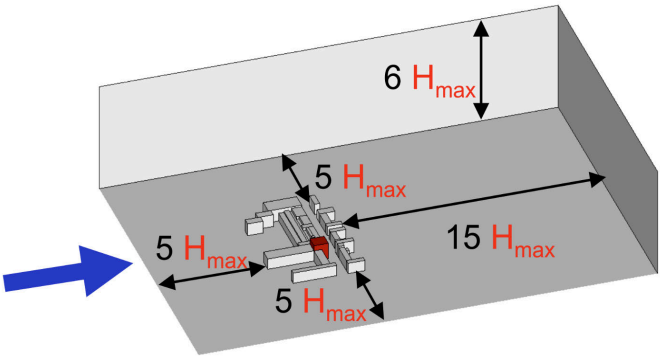


Figure. 9: Computational domain extensions according to COST

- The recommended blockage ratio (ratio of the frontal area of the building silhouette to the domain frontal area for a wind direction) values are around 5% and should not exceed 10%
- At least three cells below the pedestrian height (say, z = 1.75m) is recommended
- At least 12 wind directions should be simulated to perform the wind comfort and safety study
- To perform a yearly study, a statistical dataset from at least 30 years must be used to define the flow conditions

# Boundary conditions

As much as the quality of the mesh is important, it is also essential to use proper inlet and wall boundary conditions. Inlet boundary conditions define the properties of the fluid as it enters the domain, such as velocity, temperature, and pressure. Wall boundary conditions define the properties of the fluid as it interacts with the walls of the domain, such as the terrain and building facades. Incorrectly specified boundary conditions can lead to unrealistic or unphysical results, such as fluid flowing through solid walls or unnatural reflections of pressure waves. Furthermore, in some cases, the simulation may not converge at all if the boundary conditions are not specified correctly. Keeping these in mind, here are the recommended boundary conditions for the modified **k-ω** SST model [Bellegoni et al., 2023; Srikumar et al., 2024] used to perform a wind study of urban areas:

## Inlet boundary conditions

- Pressure : **zeroGradient** boundary condition
  - $\frac{\delta p}{\delta \bar{n}} = 0$
- Velocity : Logarithmic law profile
  - $u(z) = \frac{u^*}{\kappa} ln\left(\frac{z+z_0}{z_0}\right)$

- Turbulent kinetic energy (*k*): Linear profile from Brost and Wyngaard [Brost et al., 1978]
  - $k(z) = \frac{u^{*^2}}{2}\left(8.7 - 6\frac{z}{h}\right)$, for $z <= h$

    $k(z) = \frac{0.85u^{*^2}z}{h}$, for $z > h$

    $\frac{hf_c}{u^{*^2}} \approx 0.33$

    where h is the height of the ABL and $f_c$ is the Coriolis parameter, which can be taken as $f_c = 10^{-4}$ for a mid-latitude location
- Turbulent specific dissipation rate (ω): From Bellegoni *et al* under the assumption of production ≈ dissipation
  - $\omega(z) = \frac{k(z)}{\kappa u^*(z+z_0)}$

## Wall boundary conditions

- Pressure : **zeroGradient** boundary condition
  - $\frac{\delta p}{\delta \bar{n}} = 0$
- Velocity :
  - On the surface - No slip wall ⇒ $u_{face} = 0$
  - First cell height ($z_p$) ⇒ $u(z_p) = \frac{u^*}{\kappa} ln\left(\frac{z_p+z_0}{z_0}\right)$,

    $u^* = \beta^{*^{0.25}} k(z_p)^{0.5}$

- Turbulent specific dissipation rate (ω):
  - On the surface ⇒ **zeroGradient** boundary condition
    - $\frac{\delta \boldsymbol{\omega}}{\delta \bar{n}} = 0$
  - First cell height ($z_p$) ⇒ $\omega(z_p) = \frac{k(z_p)}{\kappa u^*(z_p+z_0)}$,

    $u^* = \beta^{*^{0.25}} k(z_p)^{0.5}$

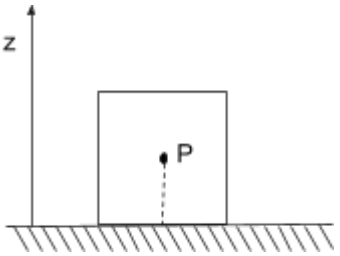

Production term ($G_{k_p}$) $\Rightarrow G_{k_p} = \tau_w \beta^{*0.25} \frac{\sqrt{k(z_p)}}{\kappa(z_p+z_0)}$

where $\tau_w$ is the shear stress on the wall

- Turbulent kinetic energy ($k$) : **zeroGradient** boundary condition
  - $\frac{\delta k}{\delta \bar{n}} = 0$

## Outlet boundary conditions

- Pressure : zero static pressure $\Rightarrow p = 0$
- All other flow quantities : **zeroGradient** boundary condition
  - $\frac{\delta f}{\delta \bar{n}} = 0$

# Validation of wind data

## Case study in Oklahoma City, USA

The area under study consisted of a circular region of radius 800m around the central business district of Oklahoma city, USA. This particular case was chosen because of the availability of experimental data from a very detailed measurement campaign performed in Oklahoma City in 2003, the Joint Urban campaign [Allwine et al., 2006], which is widely used to validate CFD wind data.

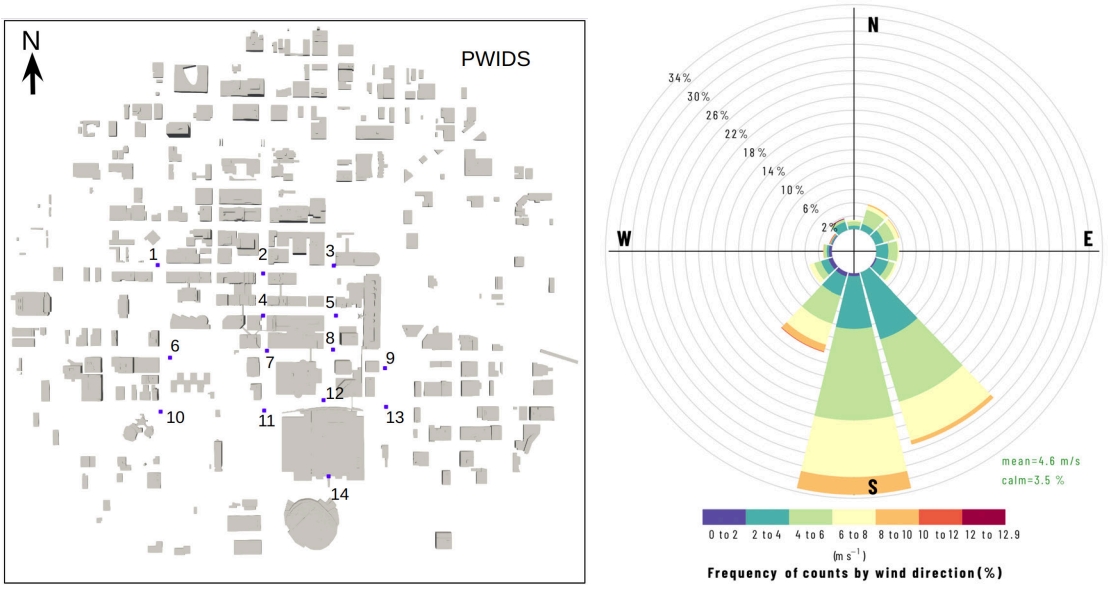


Figure. 10: CAD marked with measurement points used for validation (left) and wind rose showing the wind distribution during the measurement period (right). Refer to [Allwine et al., 2006] for details.

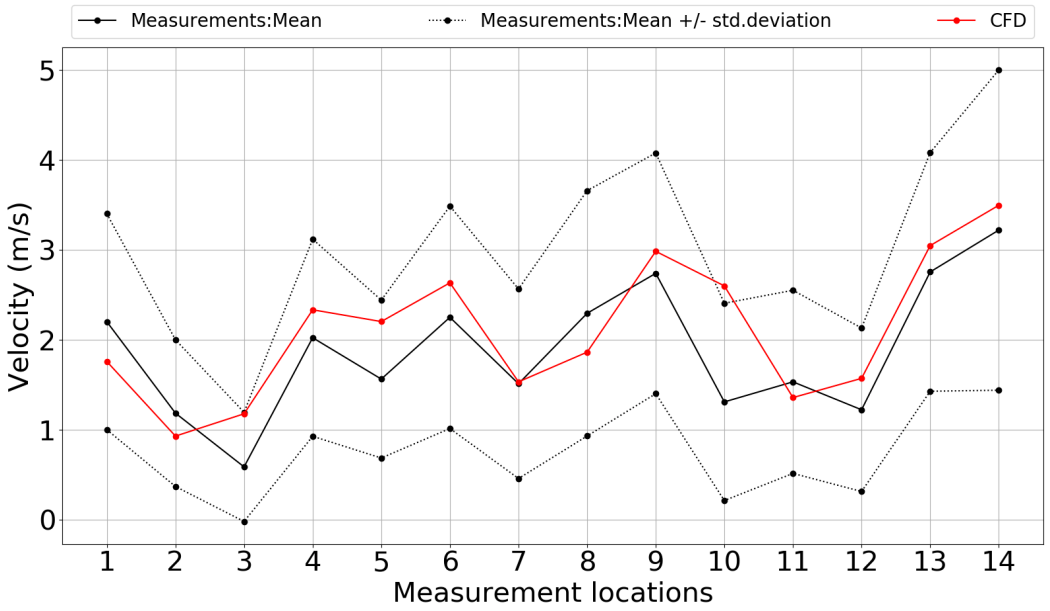


Figure. 11: Validation of CFD velocity magnitude data at the measurement locations

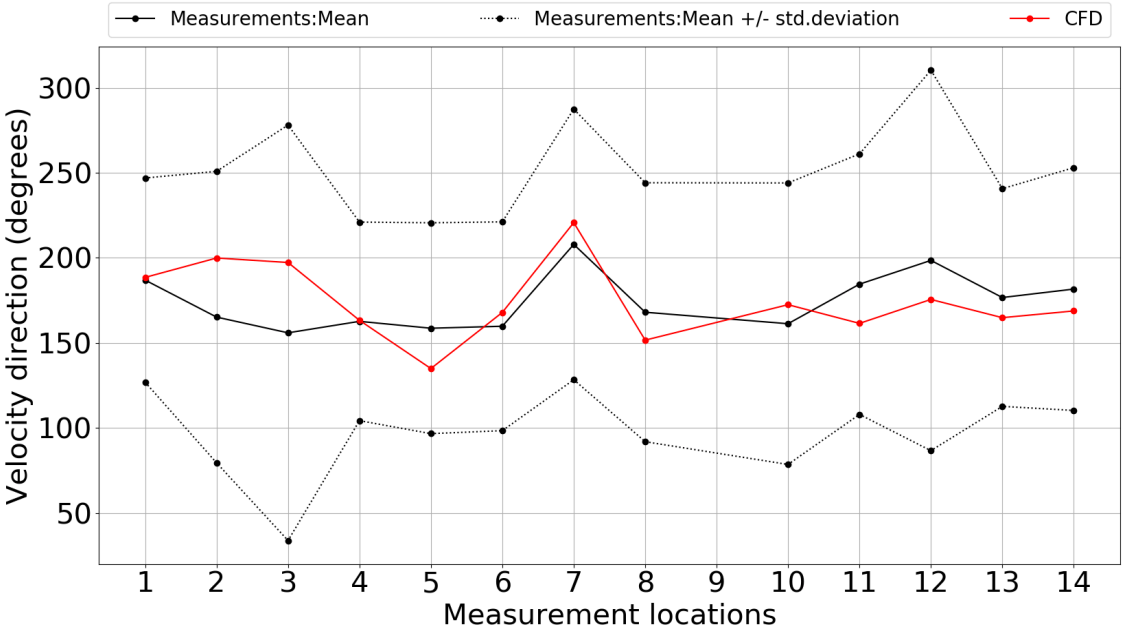


Figure. 12: Validation of CFD velocity direction data at the measurement locations

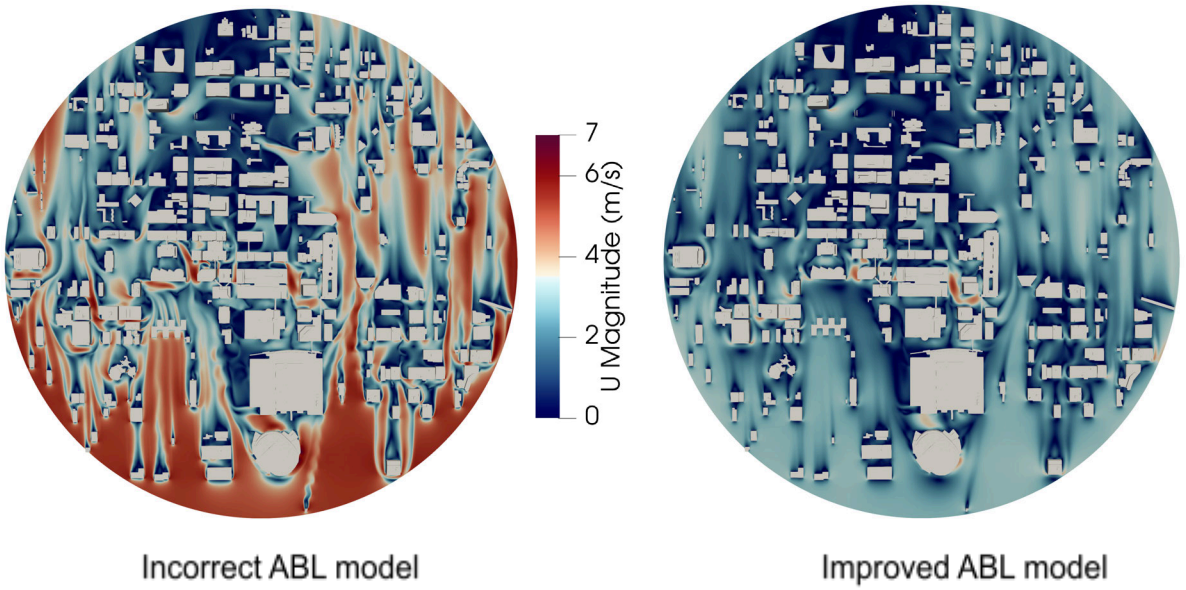


Figure. 13: Comparison of velocity magnitude obtained from an incorrect ABL model and the improved ABL model. Check [Srikumar et al., 2024] for more details.

The CFD results at nearly all measurement points fall within one standard deviation of the mean for both velocity magnitude and wind direction. The only exception is the velocity magnitude at point 10, which lies slightly outside this range; however, the wind direction at this location remains in good agreement with the measurements. Directional data for point 9 are not

presented, as the direction sensor at this location was deactivated throughout the measurement campaign due to technical issues.

The wind rose shown in Fig. 10 indicates that the most frequent wind direction corresponds to southerly flow (180°N). Consistently, the comparison of wind direction shows that the mean values are close to 180°, confirming this observation. **Overall, both velocity magnitude and direction comparisons demonstrate very good agreement with the experimental data, thereby validating the improved ABL model used in CLARA under realistic conditions.** The results of this validation study have been published in the scientific journal *Building and Environment*, and readers are referred to that article [Srikumar et al., 2024] for further details.

## Case study in ULB campus, Brussels

A network of QSENSEAIR sensors was placed around the ULB campus to monitor air quality and wind statistics in and around the campus area. At the time of the measurement campaign, three sensors were capable of providing reliable wind measurements. These three were used to validate our CFD model for wind. The velocity magnitude measurements recorded by the sensors were averaged across the entire month of March 2023 for three wind directions simulated in the CFD model: 180N, 210N, and 240N.

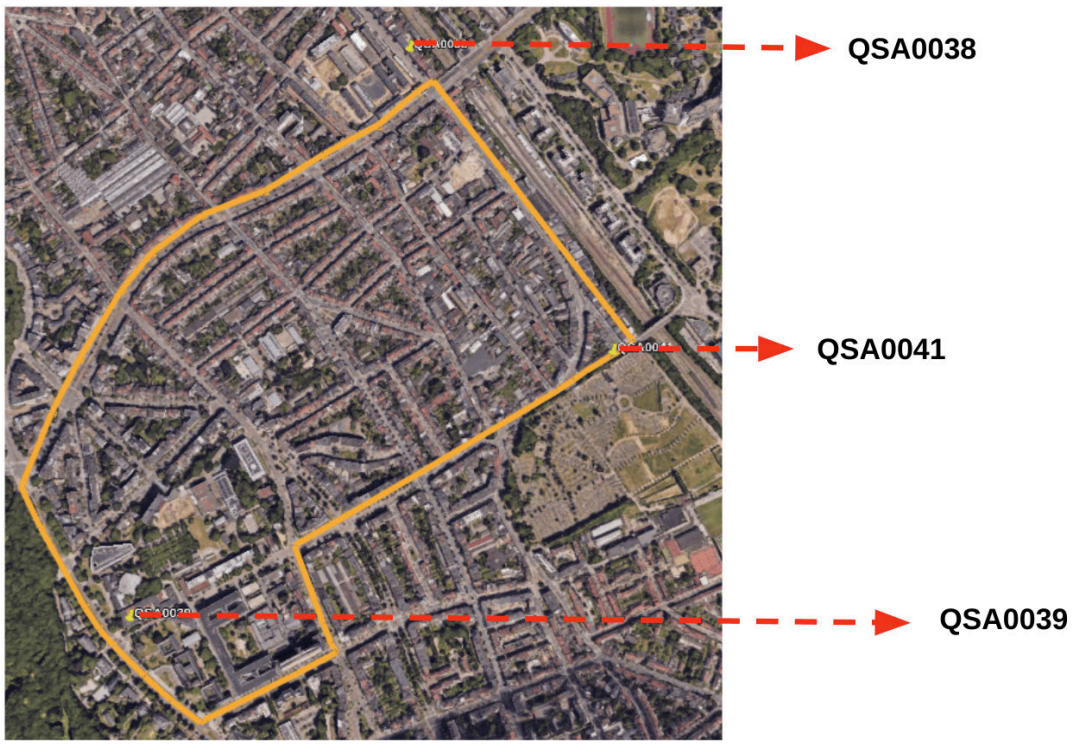


Figure 14: Locations of the three sensors installed around the ULB campus. Velocity data from these were used for validation of the CFD simulation setup.

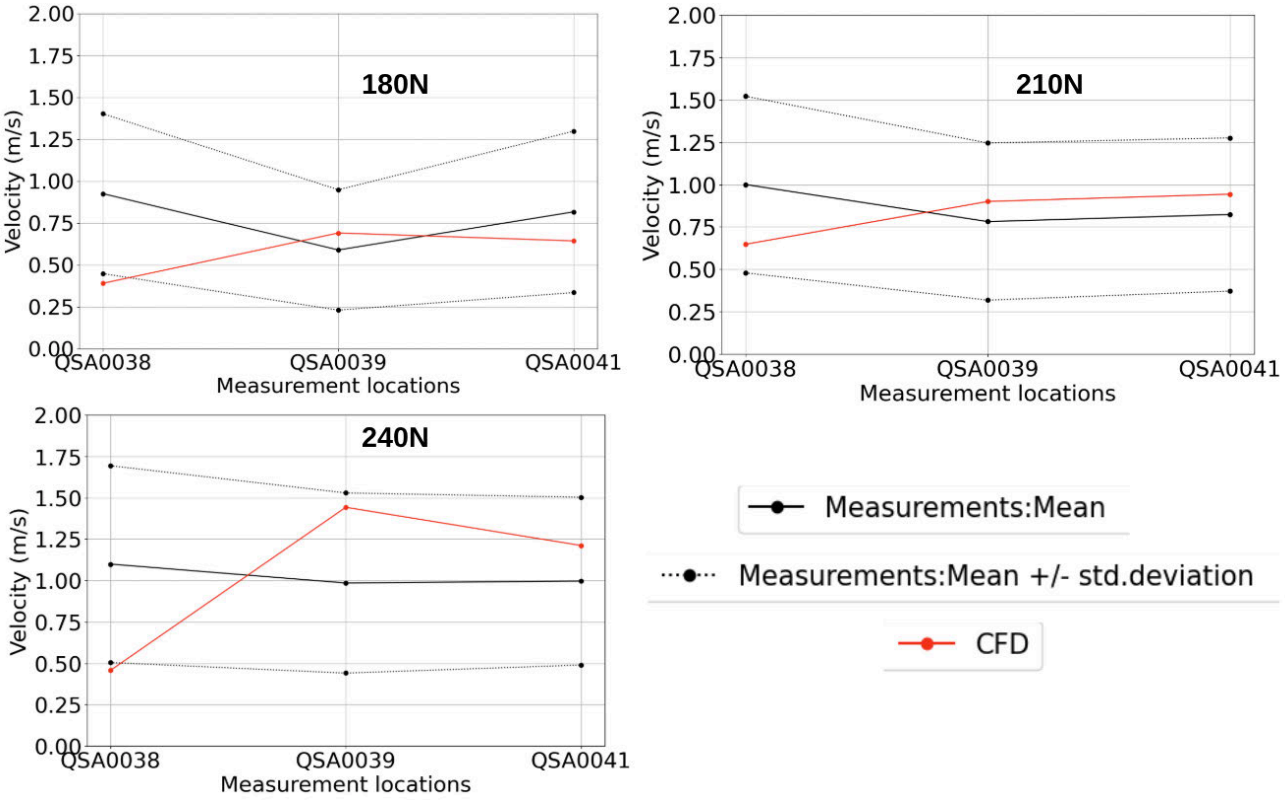


Figure 15: Validation of velocity magnitude values obtained from CFD simulations for three wind directions.

The comparison between the sensor measurements and CFD results is illustrated in Fig. 15. For sensors QSA0039 and QSA0041, the velocity magnitudes predicted by the CFD model fall within one standard deviation of the measured data across all three wind directions, indicating strong agreement and validating the simulation setup. However, for sensor QSA0038, the CFD predictions align within the standard deviation range for 210N but deviate slightly outside this range for 180N and 240N. The discrepancies observed at sensor QSA0038 can likely be attributed to localized factors. During the measurement period, ongoing construction activities were noted near the sensor's location. These temporary structures and obstructions, not accounted for in the CAD model used for the CFD setup, may have introduced localized variations in the velocity field that were not captured in the simulation. **In conclusion, the overall validation of the CFD setup demonstrates strong reliability, with minor deviations primarily attributable to external factors not included in the model geometry**.

# Methodology - Air quality estimation

## Local wind estimation

Accurately estimating pollutant concentrations at pedestrian height requires reliable knowledge of local wind conditions, as wind is the primary driver of pollutant dispersion. As discussed in the previous sections, CFD is a powerful method for capturing the complex flow patterns around urban environments, but its high computational cost makes it unsuitable for real-time prediction.

To address this, a machine learning (ML) surrogate model is developed as a fast prediction tool. Trained on a library of CFD simulations covering a range of wind speeds and directions, the surrogate learns the nonlinear relationship between inflow conditions and resulting local wind fields. Once trained, it can instantly estimate pedestrian-level wind conditions for any given boundary wind speed and direction.

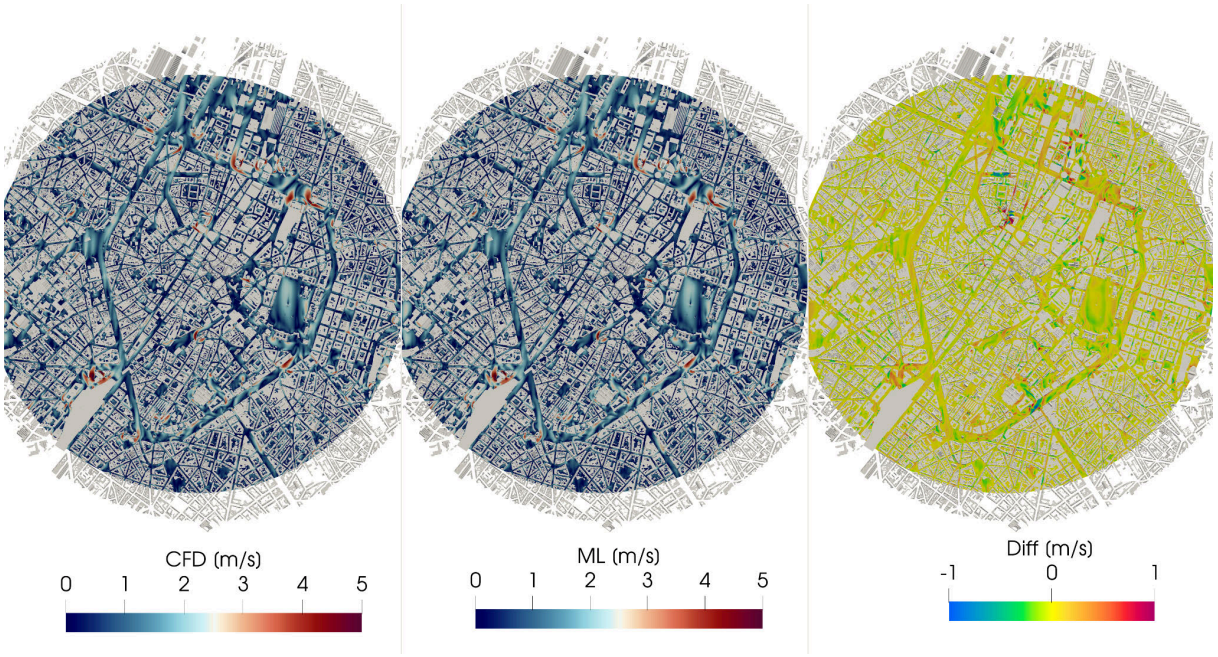


Figure 16. Example of a comparison between pedestrian-level velocities from CFD and ML, and their corresponding difference in m/s. A positive difference indicates CFD is higher.

In CLARA, this surrogate model was built on CFD results obtained using the validated CFD approach for winds, as discussed in the previous sections. The dataset included multiple wind speeds across 12 directions, from which pedestrian-height velocity fields were extracted. A deep neural network (DNN) was then trained to predict these velocities directly from the inlet flow conditions, enabling accurate and efficient real-time wind field estimation. Figure 16 illustrates a comparison between CFD and ML predictions of pedestrian-level velocities, along with their differences, while Figure 17 presents the corresponding $R^2$ error. The high $R^2$ value of 0.97 demonstrates the excellent predictive capability of the trained ML model.

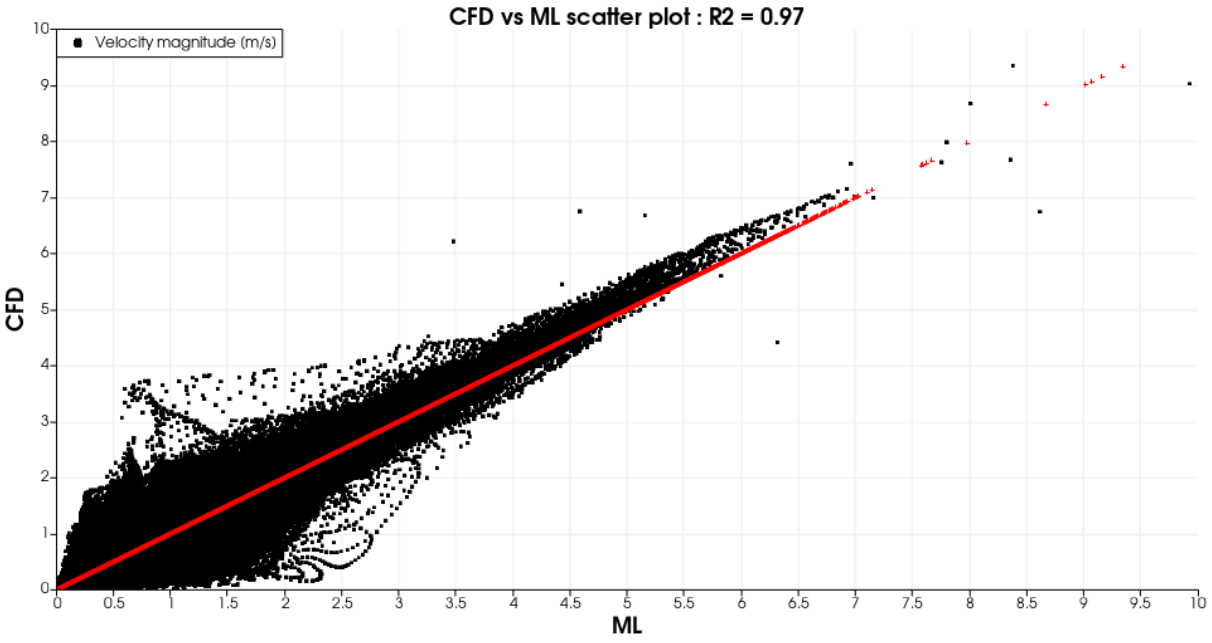


Figure 17. Scatter plot between CFD and ML velocity values from Figure.16 and their corresponding $R^2$ error.

# Pollutant source estimation

Identifying pollutant sources and their emission strengths in an urban setting is inherently challenging. The dense urban geometry, complex wind fields, and numerous potential emission sources make it difficult to accurately determine both the location and intensity of pollutants. In practice, this uncertainty limits the reliability of air quality models unless source assumptions are clearly defined. Within CLARA, pollutant sources are assumed to be fixed along the road network, reflecting traffic as the dominant contributor to urban emissions. Multiple source categories are defined to account for different road types, such as highways, arterial roads, and residential streets, each with distinct traffic densities and emission profiles. This structured representation captures the spatial variability of emissions across the city more realistically.

To estimate pollutant concentrations from these sources, CLARA employs an adjoint-based Markov Chain Monte Carlo (MCMC) method [Keats et al., 2007]. The adjoint simulations were pre-computed using the same CFD library data that was used for training the ML wind surrogate. At runtime, these adjoint fields are efficiently scaled according to the real-time local velocity predictions from the ML model. Observational data from air quality sensors from the Brussels environment agency [BEA] are then incorporated to constrain the inference process. By combining the scaled adjoint fields with the sensor measurements, the MCMC framework explores the solution space to infer the most likely source strengths for the source locations.

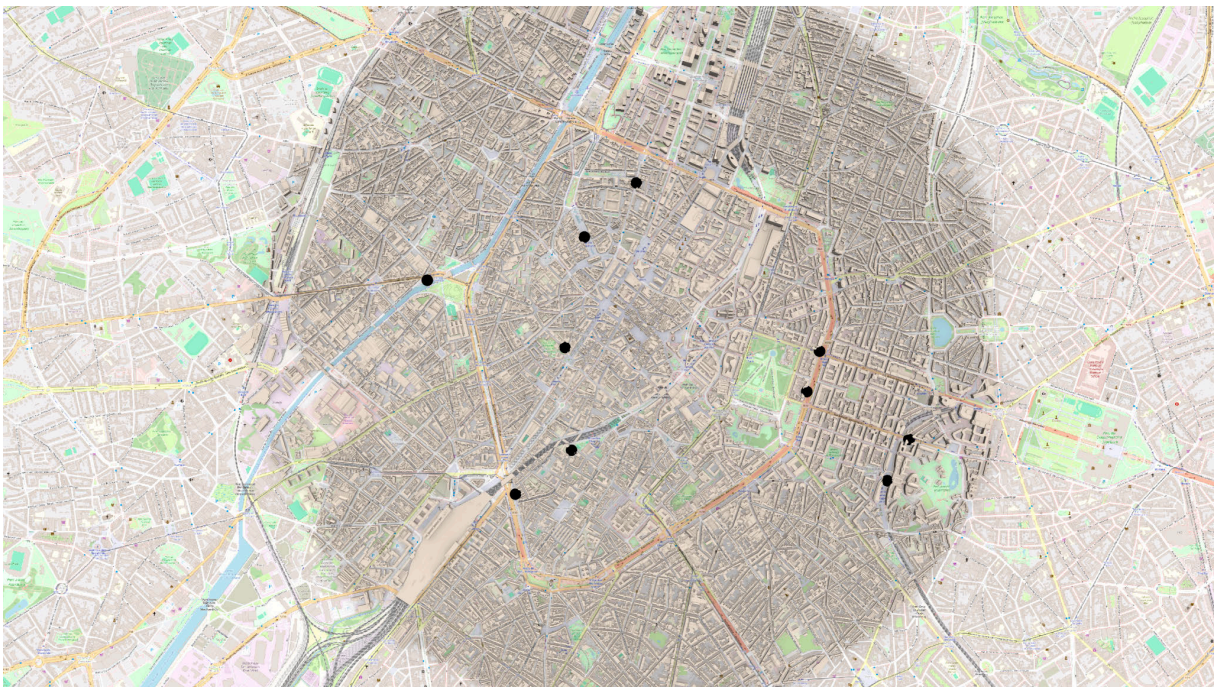

Figure 18. Location of the 10 air quality stations from the Brussels Environment agency within the territory of the City of Brussels.

## Pollutant concentration field reconstruction

Once the source strengths have been estimated, the final pollutant concentration fields across the urban domain are constructed. To achieve this efficiently, pollutant dispersion fields for unit sources are pre-computed using the same CFD library data that underpins both the ML wind surrogate and the adjoint simulations. These unit dispersion fields represent how pollutants spread through the urban environment under different inflow conditions.

At runtime, the unit fields are scaled according to two factors: the real-time local wind conditions predicted by the ML surrogate and the source strengths inferred through the adjoint-based MCMC method. This superposition approach allows pollutant concentrations to be reconstructed rapidly and accurately without requiring new CFD simulations[5].

The method relies on the assumption that pollutants behave as passive scalars, with no chemical reactions or transformations taking place. This assumption is valid at the pedestrian level for traffic-related emissions such as $NO_2$ and particulate matter, where dispersion dominates over chemical processes [Tominaga et al., 2013; Lin et al., 2022]. As a result, CLARA can generate reliable, high-resolution concentration maps that reflect both the complex urban flow structures and the dynamic influence of traffic-related emissions. An example of the constructed pollutant field is shown in Figure 19, which denotes the averaged morning rush hour $NO_2$ concentration colored by the BelAQI scale [IRCELINE] during morning rush hours.

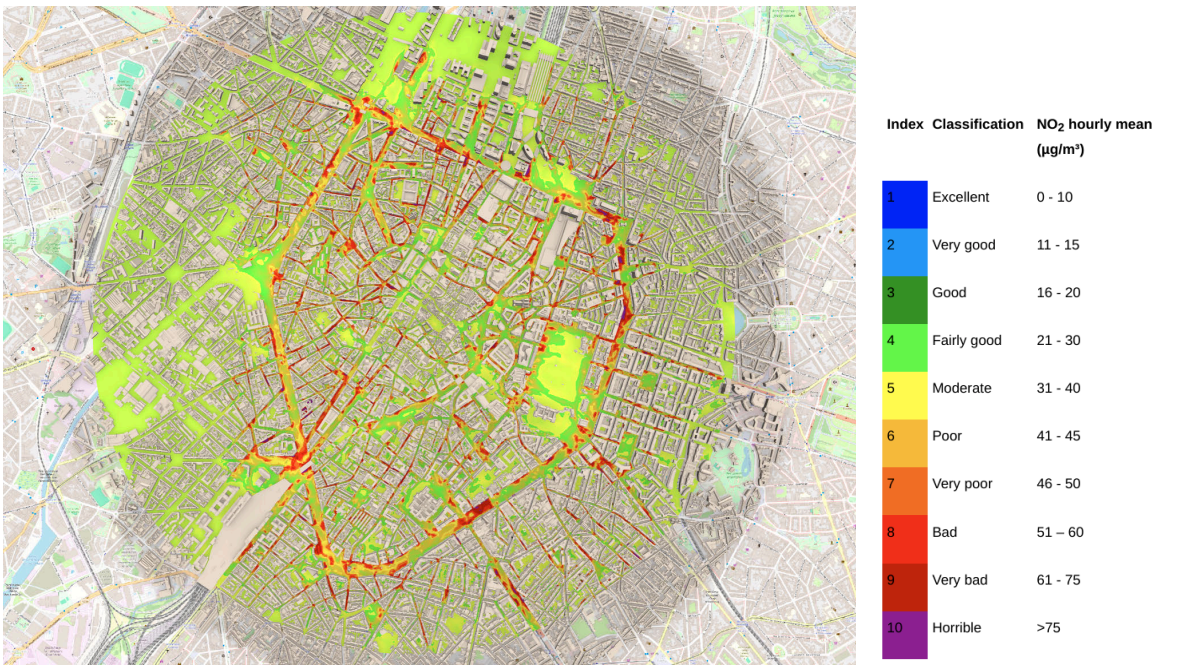


Figure 19. Example of averaged air pollution contour during morning rush hours colored according to BelAQI for $NO_2$ concentration values.

# Validation of air quality data

## Comparison with air quality monitoring stations

Model performance was evaluated by comparing $NO_2$ concentrations predicted by CLARA with observations from 10 monitoring stations operated by Brussels Environment Agency between June 1 and September 15, 2025. Concentration values were scaled using the BelAQI index (Figure 19), and the percentage of predictions within one and two BelAQI classes of the observations was calculated for each station (Figure 20).

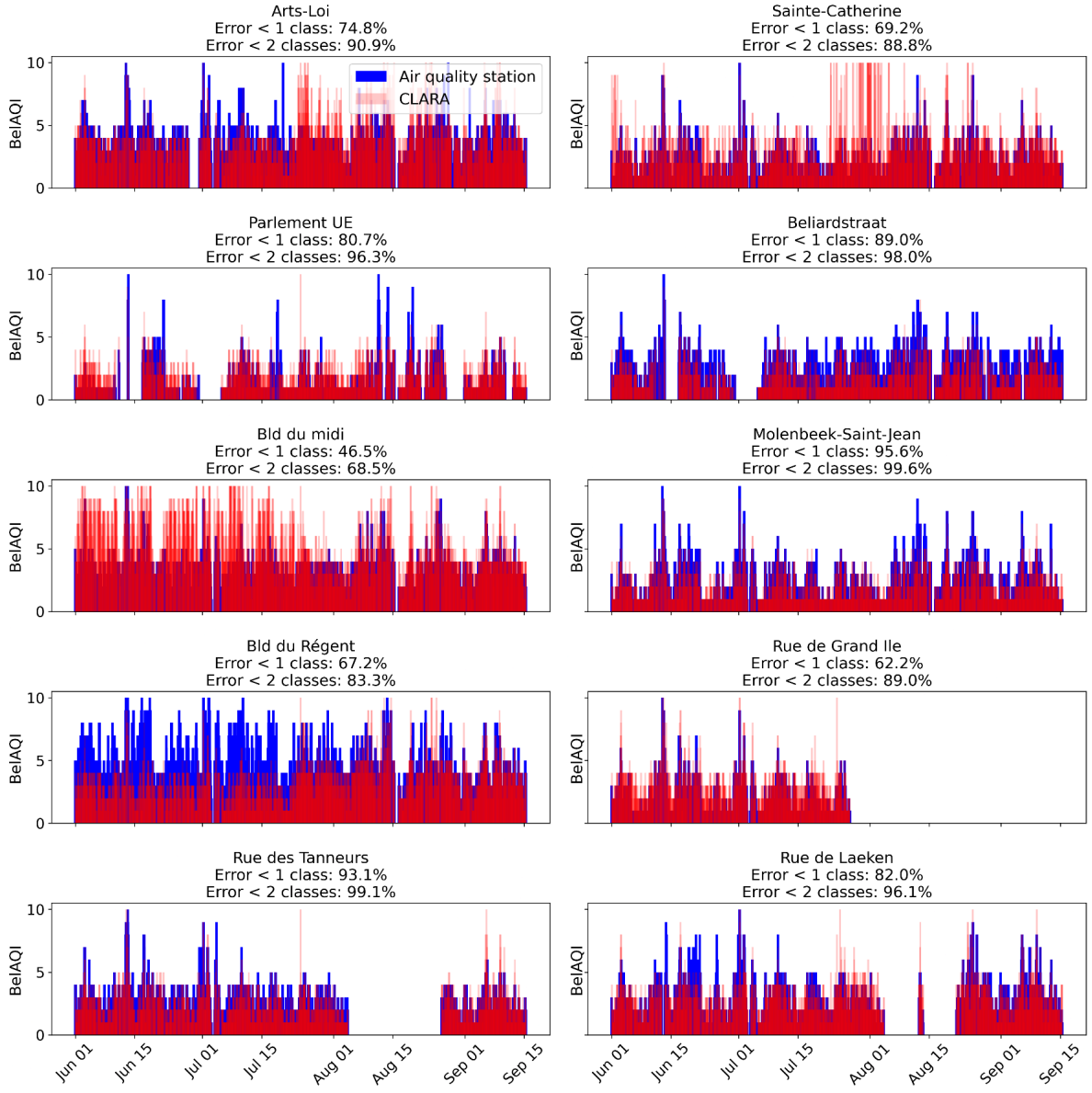


Figure 20. BelAQI comparison shown for each sensor location from Brussels Environment between $NO_2$ concentration obtained from CLARA and the air quality station. Values are scaled according to BelAQI. Percentage of predictions within one and two BelAQI classes of the observations shown for each station.

Across all stations, CLARA achieves an average accuracy of 76% within one class and 92% within two classes. Except at Boulevard du Midi, all locations exceed 80% agreement within two classes, demonstrating reliable large-scale consistency of the model. Several sites show very strong agreement, with >95% of predictions within two classes at Molenbeek-Saint-Jean (99.6%), Rue des Tanneurs (99.1%), Beliardstraat (98.0%), and Parlement UE (96.3%).

Performance within one class is naturally stricter but still encouraging. Stations such as Molenbeek-Saint-Jean (95.7%), Rue des Tanneurs (93.1%), and Beliardstraat (89.0%) indicate that **CLARA is capable of reproducing detailed temporal and spatial variations in air quality at the street scale**. Other stations, such as Sainte-Catherine (69.2%) and Rue de Grand Ile (62.2%), show reduced performance under this stricter metric, suggesting challenges in capturing finer-scale variability in complex street canyons.

In contrast, Boulevard du Midi stands out with lower accuracy (46.5% within one class, 68.5% within two). This underperformance may reflect unique local emission dynamics, traffic patterns, or complex flow structures not fully represented in the CFD library.

**Overall, the validation demonstrates that CLARA provides robust city-wide $NO_2$ predictions, with strong alignment to monitoring data** and especially high reliability under the <2 class metric. The stricter <1 class results highlight areas for refinement, while the systematic underperformance at Boulevard du Midi points to the need for targeted improvements in local source representation or flow modeling.

# Comparison with CurieuzenAir campaign data

CurieuzenAir [CurieuzenAir] was a large-scale citizen science study conducted in Brussels to map nitrogen dioxide ($NO_2$) concentrations with fine spatial resolution. The campaign ran for four weeks, from 25 September to 23 October 2021, and involved 3,000 measurement locations across all 19 municipalities of the Brussels Capital Region. Within the area of interest of CLARA, there were 491 data points (Figure 21). Note that only 6/10 sensors were operational in 2021, and only these were used to perform the calculations for comparison.

Measurements were made using passive diffusion tubes: participants (families, schools, associations, businesses) installed a small panel with two $NO_2$ sensor tubes on the street-facing side of a window (ideally on the first floor) for the duration of the measurement period. The chosen sites represented a variety of street types (busy vs. quiet roads, narrow vs. wide streets, areas with and without trees, etc.) to capture spatial contrasts in exposure. After the campaign, the tubes were collected, analysed in a laboratory, and the results were shared publicly via an interactive map. Importantly, the reported values correspond to time-averaged $NO_2$ concentrations over the four-week measurement period.

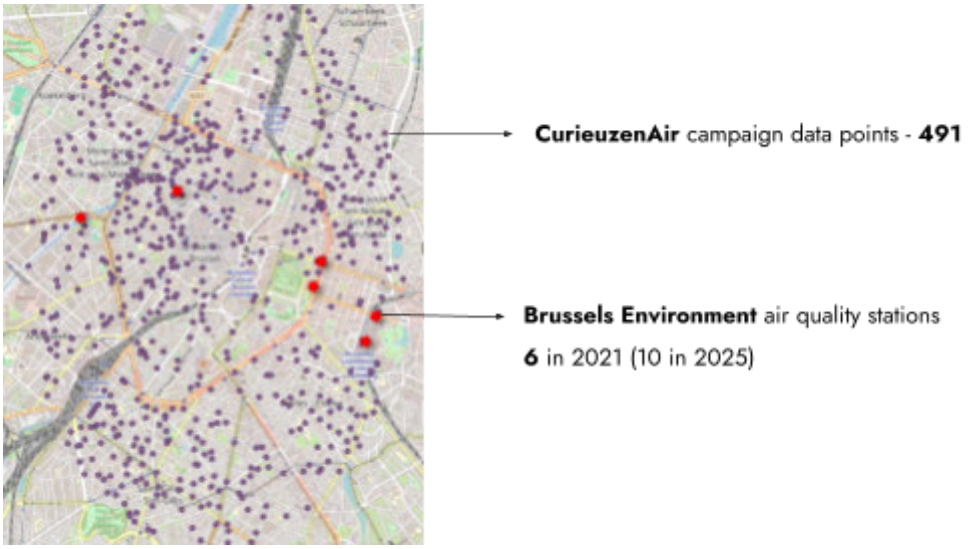


Figure 21. CurieuzenAir campaign data points within the area studies, along with the Brussels Environment air quality stations shown. Note that only 6/10 sensors were operational in 2021.

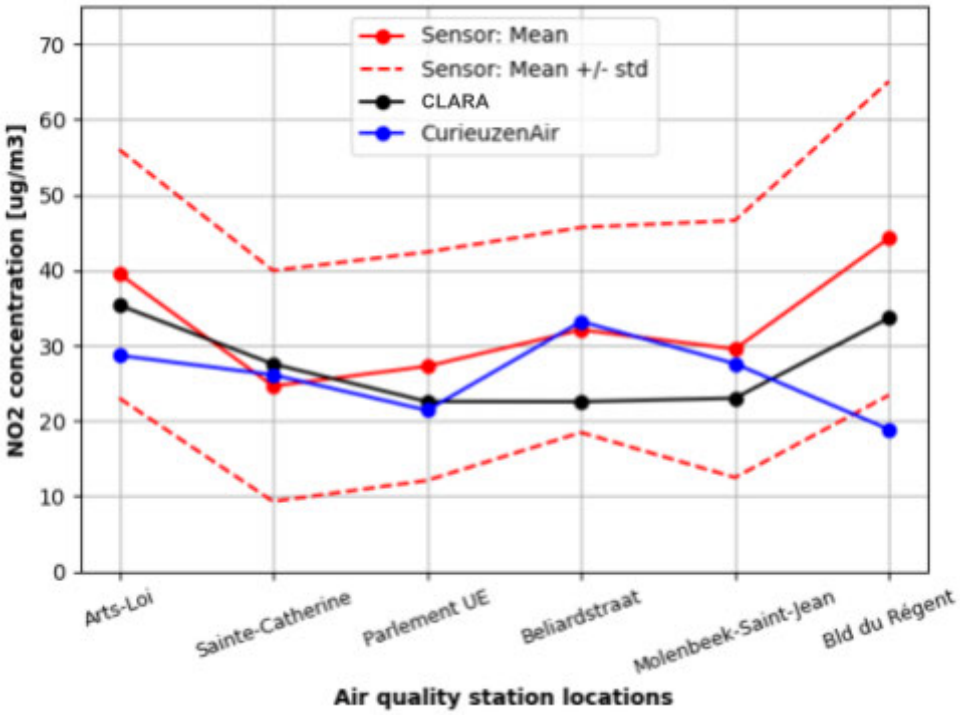


Figure 22. Comparison of averaged $NO_2$ concentration values over the CurieuzenAir campaign among the 6 air quality stations, CLARA, and CurieuzenAir data. Dotted red lines show values of Mean+/- σ, where σ is the standard deviation.

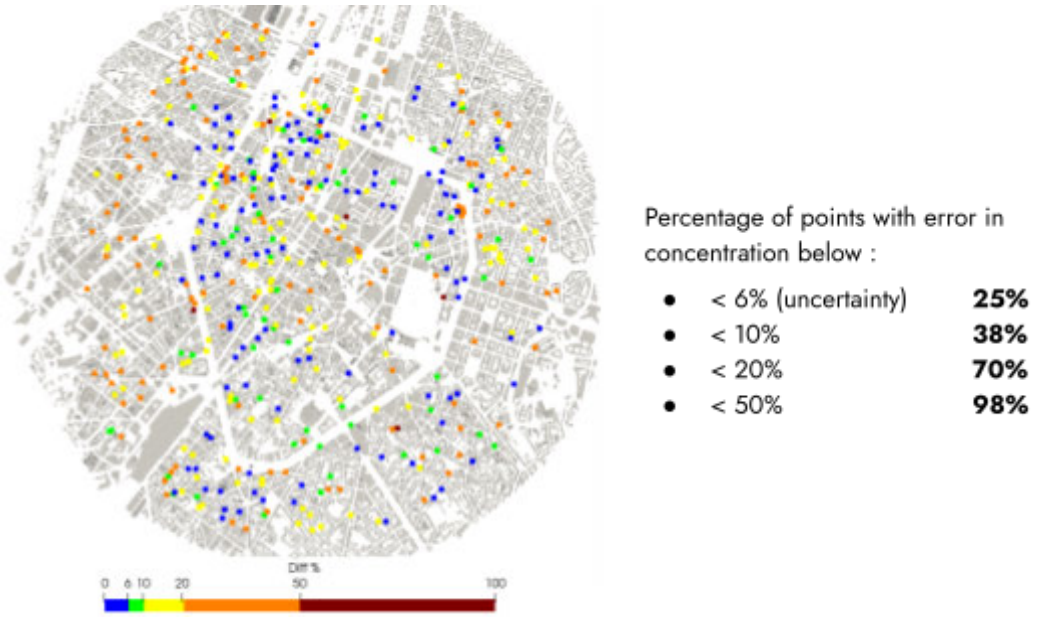


Figure 23. Percentage of CurieuzenAir data points where the errors between the averaged $NO_2$ concentrations from CurieuzenAir campaign and CLARA are below different thresholds.

Figure 22 presents the comparison of averaged $NO_2$ concentration values during the CurieuzenAir campaign across six Brussels air quality stations, CLARA predictions, and the CurieuzenAir measurements. The dotted red lines indicate the mean ± one standard deviation of the campaign results. At all locations, CLARA's predictions fall within one standard deviation of the observed means, showing good consistency with both the campaign averages and the fixed monitoring stations.

A broader comparison between CLARA and all CurieuzenAir measurement points further highlights the model's performance. The percentage of locations with concentration errors below various thresholds is:

- 25% of points within 6% error (matching the uncertainty of the passive sensors),
- 38% within 10% error,
- 70% within 20% error,
- 98% within 50% error.

These results suggest that CLARA reliably captures the spatial variability of $NO_2$ across Brussels. While only about a quarter of locations fall strictly within the inherent uncertainty of the diffusion tubes, **the vast majority (70% within 20% error) show close agreement with the campaign measurements**. The very high percentage within 50% error (98%) indicates that **systematic deviations are rare and likely limited to specific local conditions or emission hotspots** not fully represented in the model input.

Figure 23 spatially illustrates these errors across Brussels, with data points colored by their percentage difference between CLARA and CurieuzenAir values. The map highlights locations of low-error points (in blue) where CLARA predictions align well with observations, alongside spots

of higher discrepancy (orange and red). These higher-error areas could be attributed to the uncertainty in the location of the sensors used in the Campaign. While metadata may indicate positions in the middle of streets, in practice, most tubes were attached to building façades. Since CFD-based wind and dispersion fields are highly sensitive to exact position - particularly in narrow street canyons - small misalignments between reported and actual sensor locations likely explain much of the higher error spots seen in Figure 23.

# References


1. Bennett, J., 2007. Wind design guide. Architectural aerodynamics course.
2. NEN-8100. (2006). Nen 8100 : Wind comfort en wind danger in the built environment (Tech. Rep.). Netherlands Normalisation Institute.
3. London (2019). City of london wind microclimate guidelines.
4. Anderson, J.D. and Wendt, J., 1995. Computational fluid dynamics (Vol. 206, p. 332). McGraw-Hill.
5. Ferziger, J.H., et al., 2002. Computational methods for fluid dynamics (Vol. 3, pp. 196-200). Berlin: springer.
6. Pope, S.B., et al. 2000. Turbulent flows. Cambridge university press.
7. Menter, F.R., 1994. Two-equation eddy-viscosity turbulence models for engineering applications. AIAA journal, 32(8), pp.1598-1605.
8. Menter, F.R., et al., 2003. Ten years of industrial experience with the SST turbulence model. Turbulence, heat and mass transfer, 4(1), pp.625-632.
9. Blocken, B., et al., 2007. CFD simulation of the atmospheric boundary layer: wall function problems. Atmospheric environment, 41(2), pp.238-252.
10. Parente, A., et al., 2011. Improved k–ε model and wall function formulation for the RANS simulation of ABL flows. Journal of wind engineering and industrial aerodynamics, 99(4), pp.267-278.
11. Hargreaves, D.M., et al., 2007. On the use of the k–ε model in commercial CFD software to model the neutral atmospheric boundary layer. Journal of wind engineering and industrial aerodynamics, 95(5), pp.355-369.
12. Bellegoni, M., et al., 2023. An extended SST k– ω framework for the RANS simulation of the neutral Atmospheric Boundary Layer. Environmental Modelling & Software, 160, p.105583.
13. Wieringa, J., 1992. Updating the Davenport roughness classification. Journal of Wind Engineering and Industrial Aerodynamics, 41(1-3), pp.357-368.
14. WMO, G., 1996. Guide to meteorological instruments and methods of observation.
15. Gulvanessian, H., 2001, November. En1991 eurocode 1: Actions on structures. In Proceedings of the Institution of Civil Engineers-Civil Engineering (Vol. 144, No. 6, pp. 14-22). Thomas Telford Ltd.
16. Franke, J., et al., 2010. The Best Practise Guideline for the CFD simulation of flows in the urban environment: an outcome of COST 732. In The Fifth International Symposium on Computational Wind Engineering (CWE2010) (pp. 1-10).
17. Blocken, B., 2015. Computational Fluid Dynamics for urban physics: Importance, scales, possibilities, limitations and ten tips and tricks towards accurate and reliable simulations. Building and Environment, 91, pp.219-245.
18. Brost, R.A. and Wyngaard, J.C., 1978. A model study of the stably stratified planetary boundary layer. Journal of Atmospheric Sciences, 35(8), pp.1427-1440.
19. Allwine, K.J. and Flaherty, J.E., 2006. Joint Urban 2003: Study overview and instrument locations (No. PNNL-15967). Pacific Northwest National Lab.(PNNL), Richland, WA (United States).
20. Tominaga, Y. and Stathopoulos, T., 2013. CFD simulation of near-field pollutant dispersion in the urban environment: A review of current modeling techniques. Atmospheric environment, 79, pp.716-730.
21. Lin, C., Wang, Y., Ooka, R., Flageul, C., Kim, Y., Kikumoto, H., Wang, Z. and Sartelet, K., 2022. Modelling of street-scale pollutant dispersion by coupled simulation of chemical reaction, aerosol dynamics, and CFD. Atmospheric Chemistry and Physics Discussions, 2022, pp.1-32.
22. Srikumar, S.K.R., Cotteleer, L., Mosca, G., Gambale, A. and Parente, A., 2024. Application of a comprehensive atmospheric boundary layer model to a realistic urban-scale wind simulation. Building and Environment, 253, p.111330.
23. BEA - Brussels Environment Agency - https://environment.brussels/
24. IRCELINE - https://www.irceline.be/en/air-quality/measurements/air-quality-index-november-2022/info_nov2022
25. CurieuzenAir campaign - https://curieuzenair.brussels/en/home/